Optimizing Navigation Channels through Hydrodynamic and Sedimentation Modeling: A Case Study of the Barito River Estuary, South Kalimantan

Candida Aulia De Silva Nusantara[1*], *Khomsin*[1], *Muhammad* Aldila Syariz[1], *Andik* Cahyo Utomo[1], *Muhammad* Rafly Rahardian[1]

[1]Department of Geomatics Engineering, Faculty of Civil, Planning, and Geo Engineering (CIVPLAN), Sepuluh Nopember Institute of Technology, Surabaya, Indonesia
* Corresponding author: candida.nusantara@its.ac.id

Abstract. The Barito River Estuary in South Kalimantan plays a crucial role in Indonesia's maritime transportation, particularly in trade and coal transshipment. As the largest river in Kalimantan, with its estuary facing the Java Sea, it supports regional economic activities. However, channel siltation due to sedimentation presents significant challenges, exacerbated by natural changes along the river and estuary. Sediment grain size and current velocity are key factors in sediment movement. This study uses Delft3D software to model hydrodynamic and sedimentation patterns in the estuary. The model reveals significant variations in current speed and direction between tidal cycles and seasons. During the wet season, stronger currents, averaging 0.1 m/s, flow from upstream to downstream, distributing sediment more evenly across the estuary. In contrast, the dry season shows increased sedimentation, concentrating in specific areas. The sedimentation model estimates that during the dry season, sediment deposition could reach 0.100 meters over six months (0.017 meters per month), while in the wet season, it is approximately 0.060 meters over six months (0.010 meters per month). These dynamics impact navigation channels, particularly during the dry season when sedimentation narrows and shallows the channels, limiting access for larger vessels and increasing the risk of grounding. This study aligns with SDG 9: Industry, Innovation, and Infrastructure, as ensuring efficient navigation channels is vital for fostering sustainable industrial growth and improving maritime logistics.

1 Introduction

The Barito River provides easy access for transporting mining products and serves as a natural transportation route for moving coal from mining areas to their destinations. It is also an integral part of daily life for the local population [2]. Additionally, the Barito River is the confluence of several other rivers, such as the Martapura River and the Negara River. These interconnected rivers form economic and social networks between regions. The river network functions as vital transportation infrastructure, supporting both residents and mining activities [2]. Each river flows through the regency capitals, making them crucial transportation routes for daily life and regional economies [2].

An efficient navigation channel in this estuary is critical to ensuring smooth goods distribution and promoting regional economic growth. According to Syaefudin (2008), one of the primary challenges to navigation is channel sedimentation caused by siltation, which is influenced by natural changes in upstream, midstream, and estuarine areas [3]. Sediment transport is affected by current velocity and sediment grain size. Yolanda et al. (2020) stated that larger sediment grains require higher current velocity to be transported. Currents also determine the direction and distribution of sediment. This force contributes to variations in sediment characteristics, leading to diverse sediment populations on the riverbed. Coarse particles generally deposit near their sources, while finer particles are carried further downstream [4].

* Corresponding author: candida.nusantara@its.ac.id

The hydrodynamic modeling of current and sediment transport patterns can serve as a specialized approach to project management, optimize performance, and predict navigation channel efficiency for sustainable transportation [5]. Therefore, hydrodynamic modeling of currents and sedimentation is crucial to understanding the aquatic dynamics of the Barito River estuary. This study aims to provide deeper insights into how current and sedimentation patterns evolve over time in this estuary. Hydrodynamic modeling will help identify distinctive current patterns across seasons and weather conditions, while sedimentation modeling will offer insights into sediment deposition within the navigation channel.

Hydrodynamic model analysis enhances our understanding of water dynamics in the Barito River estuary, with the primary goals of improving navigation safety and transportation efficiency. Additionally, this deeper understanding supports decision-making regarding channel management, project planning, and environmental protection. Consequently, this study is expected to contribute significantly to optimizing the utilization of the navigation channel and promoting sustainable economic growth in South Kalimantan.

2 Methods

The navigation channel of the Barito River is maintained and managed to ensure the safe and efficient passage of vessels. The navigation channel is regulated under the Decree of the Minister of Transportation of the Republic of Indonesia No. KM 46 of 2023, which designates the waters of Banjarmasin Port in South Kalimantan as a Class 1 compulsory pilotage area [6]. Figure 1. Changes in river conditions, such as sedimentation or alterations in water flow, can affect the navigation channel, making continuous monitoring and maintenance necessary, especially in the river estuary.

The river estuary is the downstream section of the river that connects to the sea. Issues at the river estuary can be observed in the mouth of the river and the estuary area. The river mouth is the most downstream part of the estuary that directly meets the sea. Meanwhile, the estuary refers to the part of the river influenced by tidal fluctuations. In the estuary, tidal influences on flow circulation (velocity/discharge, water surface profile, saline intrusion) can extend far upstream, depending on tidal height, river discharge, and the characteristics of the estuary (cross-sectional flow, bank hardness, etc.). To address the issues in the Barito River estuary, a hydrodynamic modeling approach was employed [7].

The modeling was conducted using numerical methods with the Delft3D software. Two modeling scenarios were developed to represent two seasonal conditions: the wet/rainy season and the dry/drought season. The modeling period spans one month for the dry season (September 1–30, 2023) and one month for the wet season (October 1–31, 2023). To generalize the results for a single season (6 months), a morphological scale factor of 6 was applied. The modeling was also supported by relevant literature and data.

The data used in this study include both primary and secondary sources. Primary data consist of measurements of currents, tides for bathymetry, discharge, and sediment (grain size and total suspended solids). These measurements were conducted directly in the Barito River estuary, South Kalimantan, from October 17–23, 2023. Secondary data include nautical charts, river discharge data, wind data, and tidal variations observed at the stations of the Geospatial Information Agency (BIG), as well as tidal constants derived from the Tidal Model Driver 09 (TMD).

2.1 Research Location

The case study for this research is the Barito River estuary in South Kalimantan. The modeled area extends 69.20 km from the river estuary along the coastline upstream. This study focuses on the Barito River area, particularly the estuary. A detailed map of the research location is presented in Figure 1.

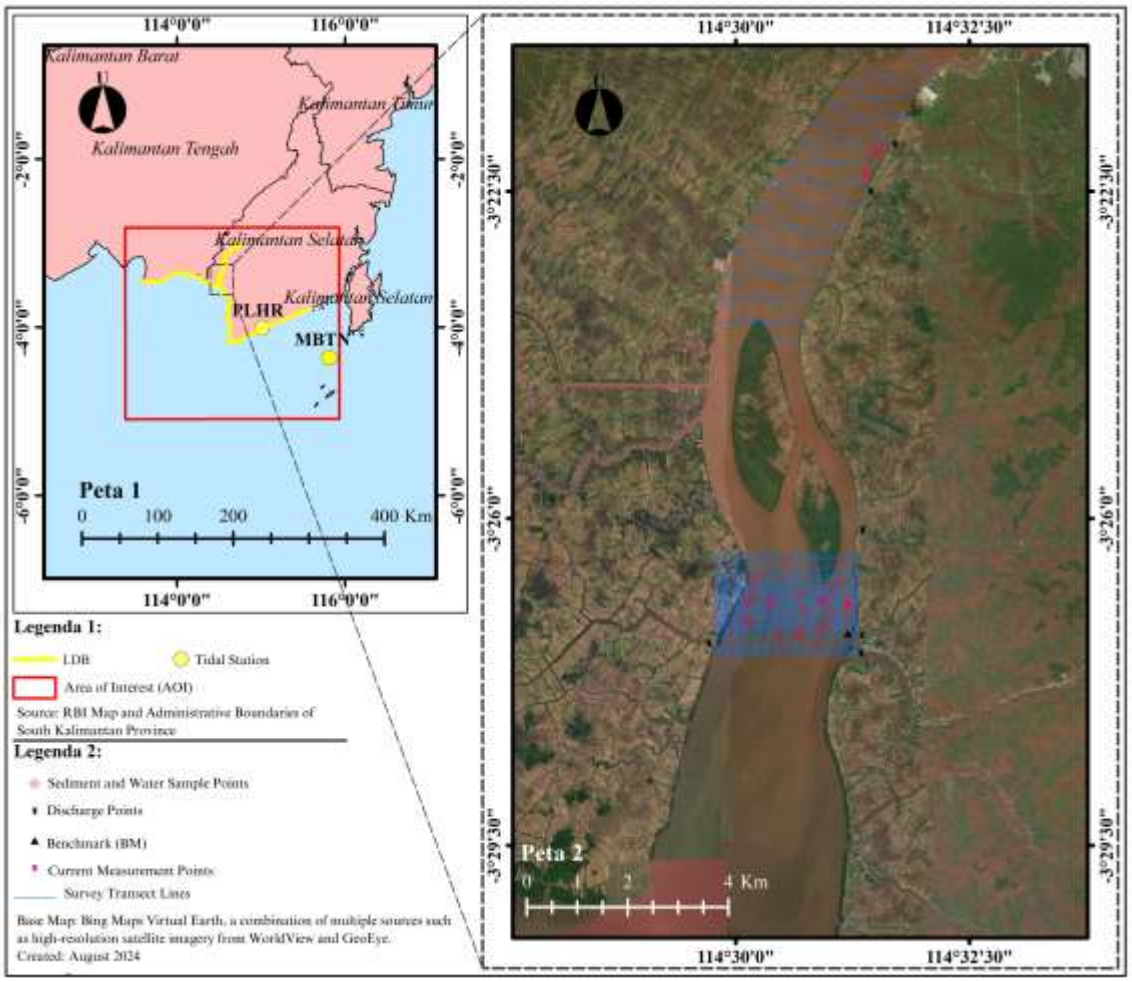

Fig. 1. Study Area located at the Barito River Estuary in South Kalimantan Province, Indonesia. This region is characterized by its complex estuarine ecosystem, influenced by both fluvial and tidal processes.

2.2 Data

Details regarding the modeling data and equipment are as follows:

2.2.1 Bathymetry Data

The bathymetry data for the Barito River estuary were obtained from both primary and secondary sources. Primary data were collected through a bathymetric survey using a Singlebeam Echosounder (SBES), with the surveyed area shown in Figure 1. Secondary data were derived from digitized nautical charts to obtain positional and depth data (xyz). Due to limitations in direct measurement coverage, secondary data from nautical charts were used to complement areas not covered by the survey. These datasets were then interpolated to create a complete bathymetric model of the study area.

2.2.2 Discharge

Discharge refers to the volume of water flowing into the river body. In an estuary, discharge flows into the river during high tide and out toward the sea [8]. The magnitude of discharge depends on the cross-sectional area of the river and the average flow velocity. The cross-sectional area is strongly influenced by river depth and width [9]. Another factor affecting discharge is rainfall, which tends to increase significantly during the wet season. High rainfall can result in the river's maximum discharge.

In a study on the Pollution Load Carrying Capacity in the Barito River Basin (including the Nagara, Marabhan, and Kuin sub-basins) in South Kalimantan Province, the maximum discharge at Station 2 (2°58'39.60"S, 114°46'14.85"E) was recorded at 379.81 m³/s [10]. Minimum discharge, on the other hand, was estimated using an approach based on the study of the Tabunio River Basin characteristics. It concluded that the ratio of maximum to minimum discharge varies from less than 20 times to more than 100 times, a characteristic of Indonesia's major rivers with moderate flood tendencies [11].

For the hydrodynamic modeling of flow and sedimentation patterns to support navigation in the Barito River estuary, primary discharge data were measured at six station points using a RiverRay ADCP, as shown in Figure 1. The detailed discharge data are presented in Table 1.

Table 1. Water discharge at each measuring station

St	Total Q	Lat (-)	Long
	(m³/s)	(DDD° MM.MMM')	(DDD° MM.MMM')
1	61.138	3 °27.429500'	114 °31.390500'
2	39.852	3 °27.285600'	114 °29.533300'
3	41.796	3 °26.123300'	114 °31.391200'
4	6.449	3 °22.507000'	114 °31.459300'
5	13.894	3 °21.998600'	114 °31.701300'
6	2.414	3 °27.240100'	114° 29.713000'

2.2.3 Currents

Currents refer to the movement of water masses [12]. They result from the movement of water masses toward equilibrium, causing both horizontal and vertical displacement of water [13]. Currents play a crucial role in sediment transport, and modeling can help identify current patterns. In this study, river current data were measured at five stations using an Aquadopp Current Profiler, as shown in Figure 2. The measured data, detailed in Table 2, were used for model validation.

Table 2. Current Measurement Results

Lat (-˚)	BT (˚)	code	Date	Time (UTC)	Speed (m/s)	Dir (˚)
3.44828	114.50632	1	19/10/2023	23:37:15	0.336	296.300
3.44828	114.50632	1	20/10/2023	06:26:13	0.396	97.718
3.44811	114.51557	2	20/10/2023	00:22:04	0.974	310.840
3.44811	114.51557	2	20/10/2023	05:44:53	0.323	261.437
3.44893	114.52005	3	20/10/2023	00:40:40	0.617	167.466
3.44893	114.52005	3	20/10/2023	06:02:50	0.537	33.532
3.37200	114.52295	4	20/10/2023	23:49:30	0.975	97.382
3.37200	114.52295	4	20/10/2023	23:50:30	1.272	89.965
3.37200	114.52295	4	20/10/2023	23:51:30	1.223	91.248
3.37200	114.52295	4	20/10/2023	23:52:30	0.993	64.183
3.37200	114.52295	4	20/10/2023	23:53:30	0.853	60.132
3.37200	114.52295	4	20/10/2023	23:54:30	0.436	83.852
3.37200	114.52295	4	20/10/2023	23:55:30	0.403	98.301
3.37200	114.52295	4	20/10/2023	23:56:30	0.393	59.777
3.37200	114.52295	4	20/10/2023	23:57:30	0.478	91.330
3.37200	114.52295	4	21/10/2023	05:51:49	0.605	58.032

Lat (-˚)	BT (˚)	code	Date	Time (UTC)	Speed (m/s)	Dir (˚)
3.37200	114.52295	4	21/10/2023	05:52:49	0.602	282.052
3.37200	114.52295	4	21/10/2023	05:53:49	0.349	211.983
3.37200	114.52295	4	21/10/2023	05:54:49	0.287	158.753
3.36784	114.52522	5	21/10/2023	00:09:09	0.306	292.739
3.36784	114.52522	5	21/10/2023	00:10:09	0.257	93.268
3.36784	114.52522	5	21/10/2023	00:11:09	0.373	65.542
3.36784	114.52522	5	21/10/2023	00:12:09	0.340	106.325
3.36784	114.52522	5	21/10/2023	00:13:09	0.368	111.728
3.36784	114.52522	5	21/10/2023	00:14:09	0.345	78.579
3.36784	114.52522	5	21/10/2023	05:38:15	0.903	238.027
3.36784	114.52522	5	21/10/2023	05:39:15	0.730	226.600
3.36784	114.52522	5	21/10/2023	05:40:15	0.477	242.634
3.36784	114.52522	5	21/10/2023	05:41:15	0.476	248.514

2.2.4 Wind

Wind is the circulation of air flowing almost parallel to the Earth's surface, driven by temperature changes. As air heats up, its density decreases, causing it to rise and be replaced by cooler air. In hydrodynamics, wind generates waves and currents [7]. Wind data were obtained from the Climate Data Store (ECMWF) website for the dry season (July–September 2023) and the wet season (October–December 2023). These data were used in modeling, including variables such as the 10m u-component of wind, the 10m v-component of wind, and surface pressure. To facilitate understanding and data visualization, wind data were exported using the Ocean Data View software and classified into wind roses using the WRPLOT software. Wind directions were categorized into eight cardinal directions: North, Northeast, East, Southeast, South, Southwest, West, and Northwest.

2.2.5 Tides

Sea level fluctuates due to periodic changes in the water surface height, known as tides. According to Poerbandono (2005), tides are periodic rises and falls in sea level caused by the gravitational forces of celestial bodies, especially the Moon and the Sun [12]. Tide data were obtained from observations at two BIG tidal stations, Pelaihari (PLHR) and Marabatuan (MBTN), for September and October 2023. The station locations are shown in Figure 1, and tidal variation graphs for September–October 2023 are presented in Figure 2.

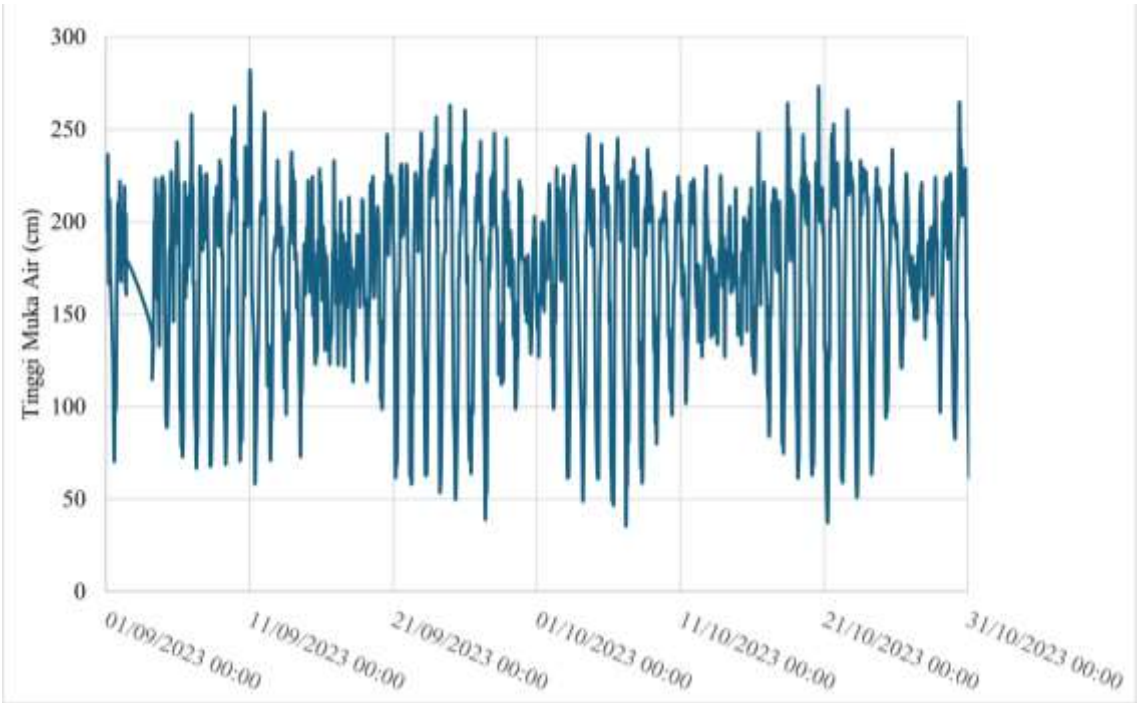

Fig. 2. Changing tides of St. PLHR September-October 2023, showing variations in sea level height throughout the period.

Tidal height data from BIG are referenced to a local datum and expressed in centimeters. However, the BIG tide observations have limitations due to non-continuous data recording.

2.2.6 Sediment

Sediment data used in this study include grain size and total suspended solids (TSS). Grain size data were obtained from bottom sediments sampled using a grab sampler, while TSS data were collected from water samples using a Nansen bottle. A total of 28 samples were collected, with sampling locations shown in Figure 1. The grain size and TSS data were analyzed in a hydrodynamics laboratory, and the results are presented in Table 3. Based on Table 3, the average values were: D_{50}: 68.831 µm, Sand: 52.665%, Silt: 42.048%, TSS: 0.074 kg/m³. The sediment laboratory test data were used as input parameters in the modeling process.

Table 3. Results Grain size and TSS data

Code	GRAIN SIZE DISTRIBUTION				TSS (kg/m³)	Lat (-˚)	Long (˚)
	D50 (µm)	Sand /Pasir (%)	Silt /Lanau (%)	Clay /Lempung (%)			
k1	84.667	63.210	32.730	4.060	0.104	3.372	114.520
k2	82.000	62.030	33.780	4.190	0.062	3.369	114.516
k3	90.667	68.190	28.300	3.510	0.060	3.368	114.506
1	74.667	55.230	39.830	4.940	0.168	3.448	114.508
2	42.733	34.380	58.380	7.240	0.124	3.448	114.515
3	78.000	59.020	36.460	4.520	0.054	3.449	114.520
4	51.833	38.550	54.670	6.780	0.042	3.454	114.520
5	96.667	78.500	19.130	2.370	0.060	3.452	114.519
6	58.667	43.410	50.340	6.240	0.074	3.451	114.518

Code	GRAIN SIZE DISTRIBUTION				TSS (kg/m³)	Lat (-˚)	Long (˚)
	D50 (µm)	Sand /Pasir (%)	Silt /Lanau (%)	Clay /Lempung (%)			
7	36.000	31.610	60.840	7.550	0.058	3.449	114.517
8	36.000	48.230	46.060	5.710	0.072	3.445	114.517
9	79.333	58.750	36.700	4.550	0.074	3.441	114.516
10	74.333	57.350	37.950	4.710	0.078	3.446	114.514
11	81.667	60.600	35.050	4.350	0.068	3.450	114.511
12	96.667	76.680	18.960	2.350	0.068	3.453	114.512
13	81.667	56.310	38.870	4.820	0.042	3.456	114.508
14	88.333	66.330	29.950	3.710	0.034	3.454	114.512
15	80.000	60.420	35.220	4.370	0.036	3.449	114.511
16	100.333	72.120	24.800	3.080	0.068	3.457	114.509
17	69.333	50.740	43.820	5.430	0.056	3.453	114.504
18	69.333	51.370	43.260	5.370	0.054	3.447	114.503
19	41.500	34.520	58.260	7.220	0.042	3.441	114.503
20	64.333	46.120	47.930	5.940	0.036	3.444	114.502
21	39.367	33.230	59.400	7.370	0.126	3.448	114.502
22	64.000	45.460	48.520	6.020	0.090	3.445	114.503
23	63.333	43.480	50.290	6.240	0.126	3.448	114.523
24	40.833	34.250	58.500	7.250	0.093	3.451	114.524
25	61.000	44.520	49.350	6.120	0.096	3.452	114.525

2.3 Data Processing

The hydrodynamic modeling of current and sedimentation patterns in the Barito River estuary requires a systematic and comprehensive data processing approach to produce accurate outputs. The research implementation includes several stages: problem identification, literature review, data collection, hydrodynamic modeling, data integration, validation, and analysis. Field survey data and secondary sources are processed using Delft3D-FLOW software to simulate current dynamics and sediment distribution. The objective is to identify flow and sedimentation patterns affecting the navigation channel in the river estuary and to provide appropriate recommendations for navigation channel management and maintenance. Consequently, the data processing stage plays a crucial role, ensuring that each variable contributing to the hydrodynamic and sedimentation conditions in the Barito River estuary is analyzed thoroughly. The data processing stage is presented in Figures 3 and 4.

Modeling essentially involves building a domain and inputting hydro-morphodynamic data into the model [14]. The main stages in model design using Delft3D-FLOW include GRID, FLOW, and QUICKPLOT. The GRID submenu consists of tools such as RGFGRID and QUICKIN. RGFGRID is used to create grids, which are spatial representations of the study area divided into small elements or cells. These grids serve as the basis for calculating changes in hydrodynamic variables, such as flow velocity, water level, and pressure distribution across the study area. Delft3D supports various types of grids, each with specific characteristics and uses. Among them is the curvilinear grid, a type of computational grid in which the cells are structured but follow curved, non-orthogonal lines, conforming to the natural geometry of the study area. This allows grid cells to align with features such as curved coastlines or meandering rivers, enhancing modeling accuracy in areas with complex topography. This study uses regular curvilinear grids, with the determination of the Area of Interest (AOI) as the initial step in modeling.

QUICKIN is a tool used to integrate bathymetry and grids, resulting in a .dep file. It also interpolates uneven or incomplete data to produce a continuous and consistent dataset on the grid for use in the model [14]. The FLOW submenu is used to create running and analysis files. Modeling can be initiated using the flow input and start tools, which support a nesting modules. In hydrodynamic modeling, nesting refers to the integration of models with varying spatial resolutions to effectively capture processes occurring at different scales. This technique allows for the refinement of simulations in specific areas of interest while still considering the broader dynamics of the entire system. The flow input tool allows hydro-morphodynamic

data to be entered into the model. It enables combining a coarse-resolution large-scale model with a fine-resolution small-scale model, allowing for more detailed analysis of specific areas without compromising broad regional coverage [14].

QUICKPLOT is the visualization module in Delft3D, used to analyze and display hydrodynamic simulation results. This module enables users to create various graphs, maps, and animations from simulation data, facilitating interpretation and further analysis. The visualized results can be presented in 2D and 3D and include temporal data.

Once the data is visualized, the next step is validation. Validation is a critical process in hydrodynamic modeling to ensure that the developed model is accurate and reliable. In Delft3D, validation involves comparing model results with field observation or experimental data to evaluate how well the model represents actual conditions.In the nesting 1 modeling stage, validation involves comparing water level model results with observation data from BIG. The statistical analyses used include Root Mean Square Error (RMSE), Mean Absolute Percentage Error (MAPE), and correlation testing.

RMSE measures the error between predicted and observed values. It is calculated as the square root of the mean squared differences between predicted and observed values, producing an absolute error value that accounts for weight. MAPE provides a relative error value, useful for assessing prediction accuracy in terms of percentage error. However, MAPE is unsuitable for data with zero values or large variations, as it can yield infinite or undefined results if actual values are zero [15]. MAPE criteria are categorized as follows: Less than 10%: Very good, 10–20%: Good, 20–50%: Fair, more than 50%: Poor [16].

Formulations for RMSE and MAPE are as follows:

$$RMSE = \sqrt{\sum_{i=1}^{N} \frac{(xi-yi)^2}{N}} \quad (1)$$

$$MAPE = \frac{1}{N} \sum_{i=1}^{N} \frac{|xi-yi|}{xi} \quad (2)$$

Where:
N: Number of observations
xi: Actual tidal value (m) from BIG observations
yi: Modeled tidal value (m)

Correlation measures the direction and strength of the linear relationship between two quantitative variables. It is denoted by **r**, ranging from -1 to +1. A correlation of 0 indicates no relationship, while positive and negative values indicate positive and negative relationships, respectively.
The correlation formulation is as follows:

$$r = \frac{1}{n-1} \sum \left(\frac{xi-\bar{x}}{s_x}\right)\left(\frac{yi-\bar{y}}{s_y}\right) \quad (3)$$

Where:
$\bar{x}$: Mean of variable x (BIG tidal observation)
$\bar{y}$: Mean of variable y (modeled tide)
s_x: Standard deviation of variable x
s_y: Standard deviation of variable y

3 Result and Discussion

3.1 Wind Analysis

Wind data were processed and analyzed to calculate the frequency and percentage of wind and wave occurrences based on wind direction classifications: North, Northeast, East, Southeast, South, Southwest, West, and Northwest. The data were visualized in a windrose diagram for the reviewed months, divided into two seasons. Dominant wind directions during the dry season came from the southeast, with wind speeds ranging from 2.10–5.70 m/s. In contrast, during the wet season, wind speeds varied from 0.50–5.70 m/s with more diverse wind directions. Figure 3.

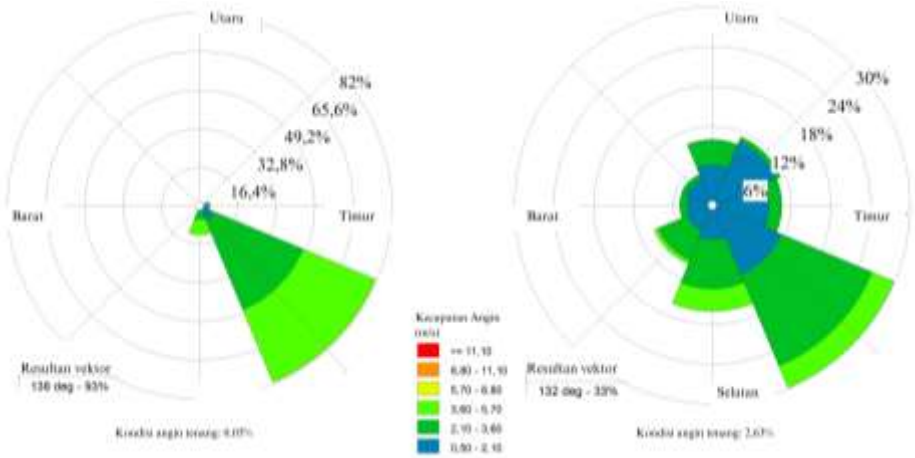

Fig. 3. Windrose in September and October showing wind direction and speed distribution, with predominant winds from the East and South during the respective months.

3.2 Tidal Analysis

The tidal observation data from BIG were used for validation. The BIG tidal observation values served as actual/reference values that closely approximate the real changes in sea surface elevation in the study area. A statistical review of the BIG tidal observation data was conducted, and normal distribution analysis was performed in this study. A normal distribution is fully determined by the mean and standard deviation. The mean, denoted as μ, is the center of the distribution, also known as the average value. In a normal distribution, the mean is the point where the data distribution is centered and forms the peak of the curve [18]. The standard deviation, denoted as σ, measures the spread of the data from the mean and indicates how much the data deviates from the mean [18].

In this study, the range of μ-σ to μ+σ was used, with the goal that approximately 68% of the data falls within one standard deviation of the mean. The standard deviation was calculated based on hourly data groups, and data checking was conducted for each hourly group, as shown in Table 4. The data were then sorted within the range of μ-σ to μ+σ. Plots of the tidal data and the corrected data can be seen in Figures 11, 12, 13, and 14 (corrected BIG).

Table 4. Calculation of the standard deviation of observation data for September-October 2023

Hur	St. PLHR			St. MBTN		
	N	*Mean*	*StDev*	N	*Mean*	*StDev*
0	28	269	31.300	56	287.520	32.270
1	30	256	30.530	57	272.960	31.760
2	30	236	29.610	60	254.920	33.060
3	30	223	33.770	58	237.240	35.790
4	28	213	36.630	57	225.510	35.560
5	31	214	38.740	60	219.800	38.310
6	31	217	41.110	60	220.120	39.910
7	31	230	44.700	60	226.880	45.130
8	29	247	43.250	59	238.710	42.540
9	30	266	41.920	57	255.040	41.910
10	30	282	39.570	58	267.980	42.530
11	30	294	38.650	60	276.250	42.990
12	29	299	34.080	57	281.980	39.950
13	28	299	30.750	54	283.980	39.480
14	29	296	27.240	56	280.480	36.960
15	29	294	22.900	57	281.390	30.730
16	30	291	16.560	58	278.600	26.820
17	30	288	14.940	59	277.080	22.440
18	29	290	11.700	59	283.170	20.520
19	29	295	10.070	56	289.160	13.080
20	30	298	9.320	58	296.860	10.980
21	30	298	12.540	60	303.720	12.210
22	30	295	20.690	59	304.390	21.990

Hur	St. PLHR			St. MBTN		
	N	*Mean*	*StDev*	N	*Mean*	*StDev*
23	29	284	27.750	57	297.930	27.520

3.3 Hydrodynamic Modeling

In this study, the hydrodynamic model uses an open boundary condition (open sea) with input data from astronomical tidal constituents, and it is constructed to align with the land boundary of the coastline and river. The grid design consists of two models: an overall model and a detailed model. The overall model grid has a resolution of 50x50 m and extends into the sea with an outer resolution of 200x200 m, as shown in Figure 4. Meanwhile, the detailed model area has a grid resolution ranging from 16x16 m to 20x20 m, as shown in Figure 5.

In the context of Delft3D, the water depth map is a visual or numerical representation of the water depth, integrated with the model grid and the processed bathymetry results, as seen in Figures 9 and 10. Bathymetry fundamentally affects water flow. The contours and depths of the seabed influence the speed and direction of water flow. Different water depths will affect the distribution of hydrostatic pressure. This pressure is crucial for determining the vertical and horizontal movement of water. The shape of the seabed affects how sediments and pollutants move and accumulate [14]. For instance, areas with slow flow tend to be places where sediment is deposited [19].

The modeling simulation was carried out with two scenarios: the dry season and the wet season. To ensure continuity between the dry season and wet season results, the modeling scheme was conducted during the transition period, with the initial run in the dry season, followed by a continuation in the wet season to ensure continuity in the initial condition usage. The initial condition is the starting condition that includes various physical parameters required to begin hydrodynamic simulations, such as water surface elevation, sediment, and temperature [14]. The initial condition scheme can be applied using restart files or map files, as shown in Figures 4 and 5. The running process is always stepwise because each output generated is used for the model in the next scheme, as shown in Figures 8 and 9.

Fig. 4. Overall Model Grid Design, which covers the Barito River, the Barito River Estuary, and parts of the surrounding waters in South Kalimantan Province.

Fig. 5. Details of the model grid design, focusing on the Barito River Estuary with smaller grid sizes to capture finer spatial resolution.

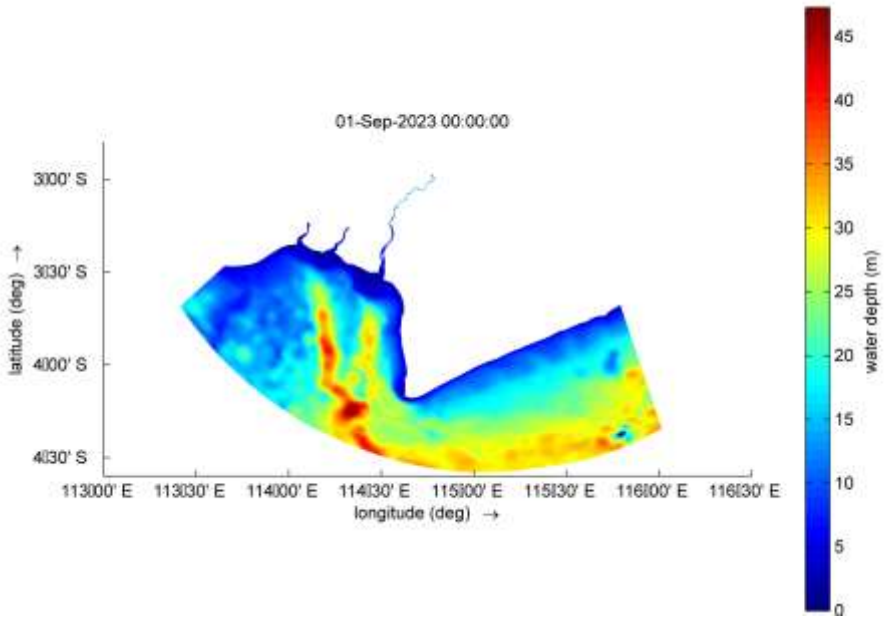

Fig. 6. Depth Map Representation of the Overall Grid Model

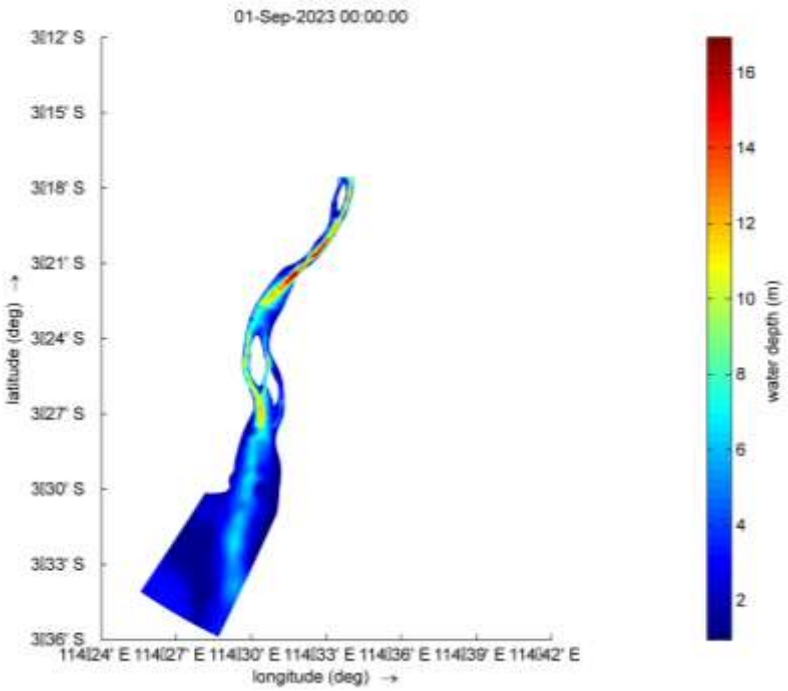

Fig. 7. Depth Map Representation of the Detailed Grid Model

After conducting hydrodynamic modeling, water level values were obtained, representing tidal phenomena across the entire modeling domain. This phenomenon reflects the dynamics of sea water influenced by gravitational forces from the moon and the sun, as well as local conditions such as bathymetry and regional morphology. Additionally, the modeling produced Total Suspended Solids (TSS) values distributed spatially throughout the domain. These TSS values indicate the concentration of suspended materials in the water, which can be used to understand sedimentation patterns and water quality during both the dry and wet seasons. The water level results at the Pelaihari Tidal Station (PLHR) are shown in Fig. 8, while the TSS results in the estuarine area are presented in Fig. 9.

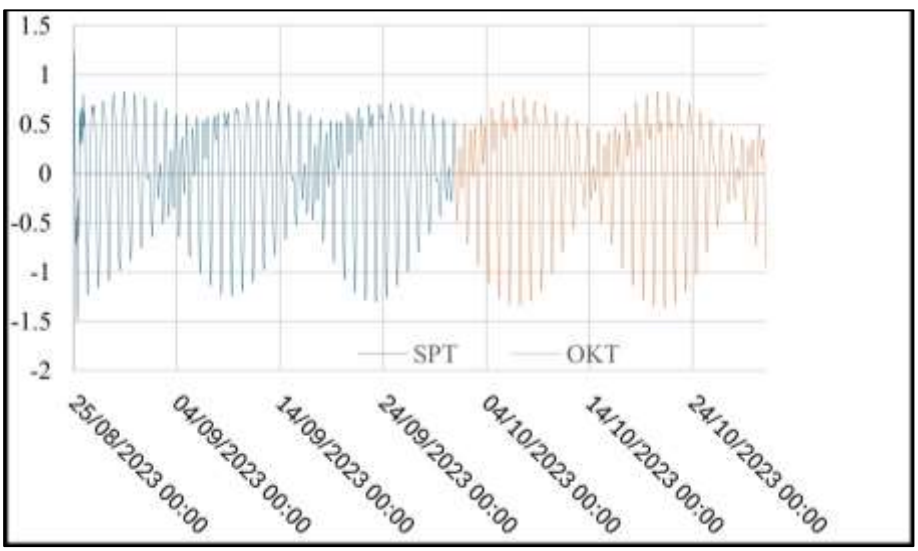

Fig. 8. Water level results from the overall dry season and wet season models at St. PLHR, based on hydrodynamic modeling. These results will be used to validate tidal observations from the tidal station operated by BIG.

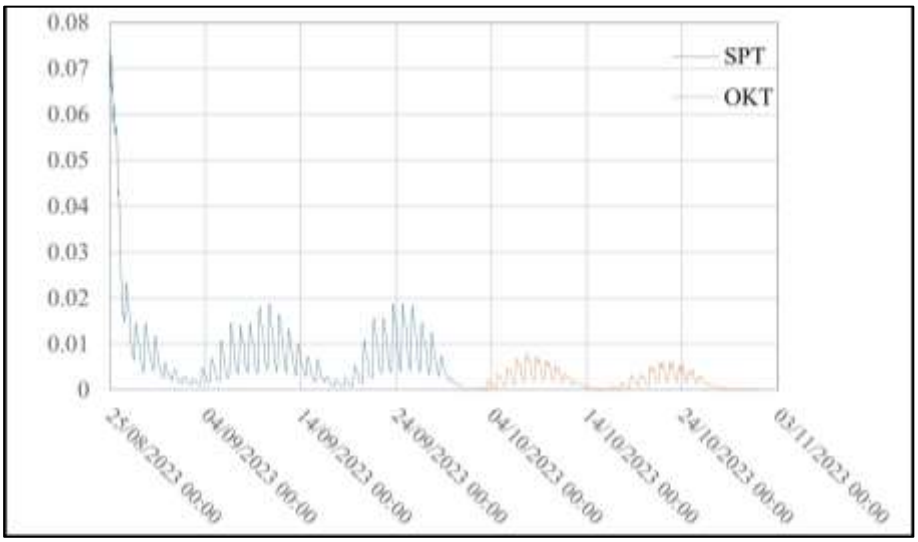

Fig. 9. TSS changes with a view to St. PLHR overalls for dry season and wet season models, showing daily fluctuations in TSS values.

3.4 Tidal Validation

The simulated water surface elevation was verified against the tidal water surface elevation data from the BIG Station, conducted over a month (September 1 - October 31, 2023). The simulated water surface elevation, shown in Figures 10, 11, 12, and 13, correlates well with the tidal data from the BIG Station, with a correlation coefficient ranging from 0.90 to 0.91, and the smallest RMSE value obtained was 0.182.

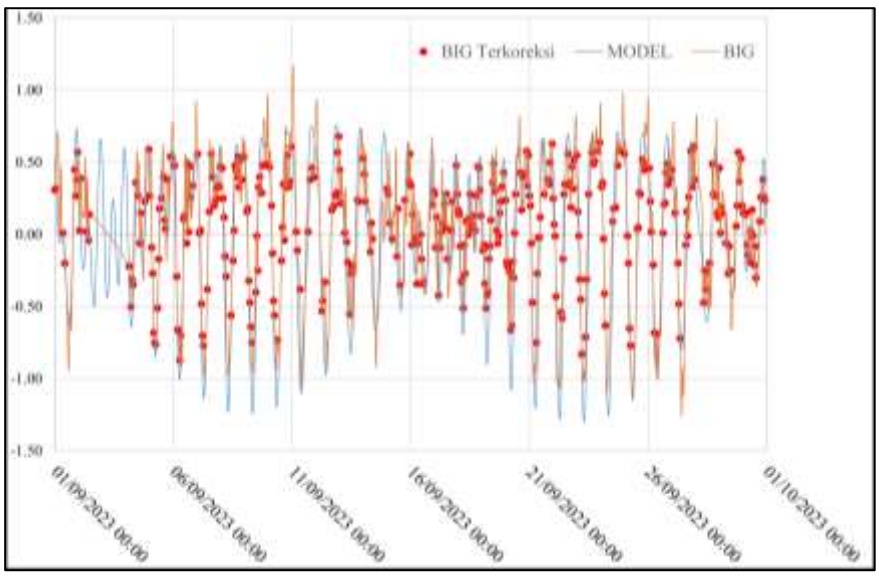

Fig. 10. Comparison of Model and Measurement Water Level Results. St. PLHR September. r=0.90, RMSE=0.226, MAPE= 8.316 %

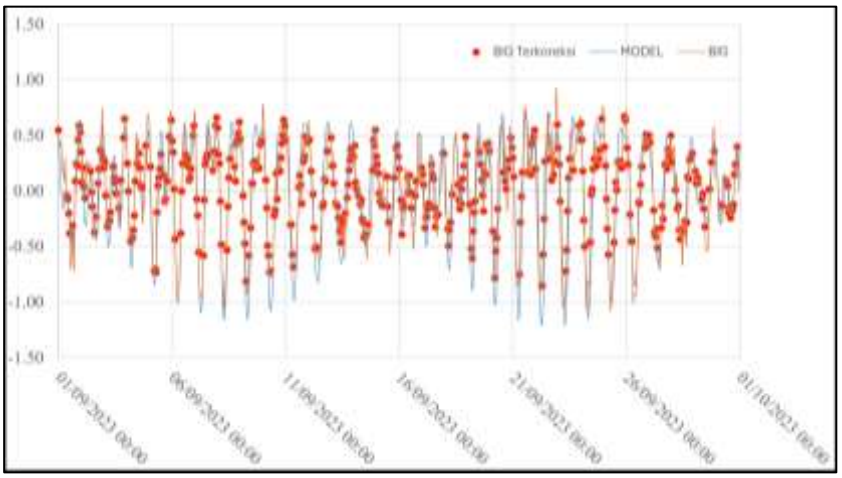

Fig. 11. Comparison of Model and Measurement Water Level Results. St. MBTN September. r=0.91, RMSE=0.186, MAPE= 5.350 %

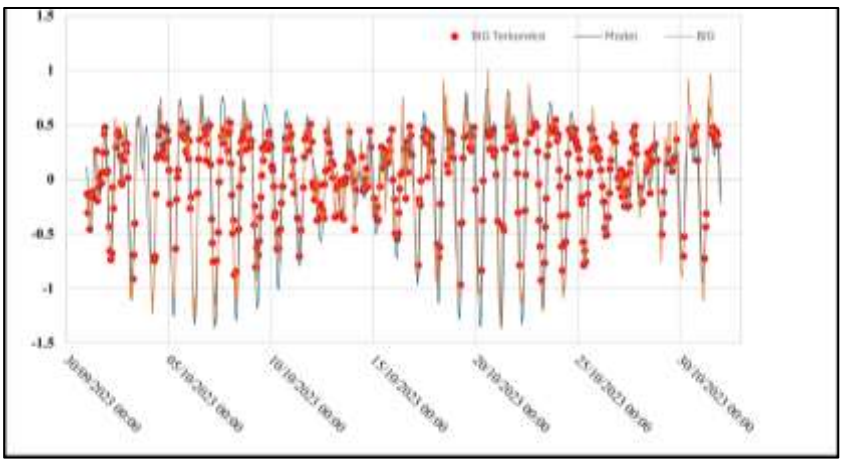

Fig. 12. Comparison of Model and Measurement Water Level Results. St. PLHR October. r=0.91, RMSE=0.191, MAPE= 5.799 %

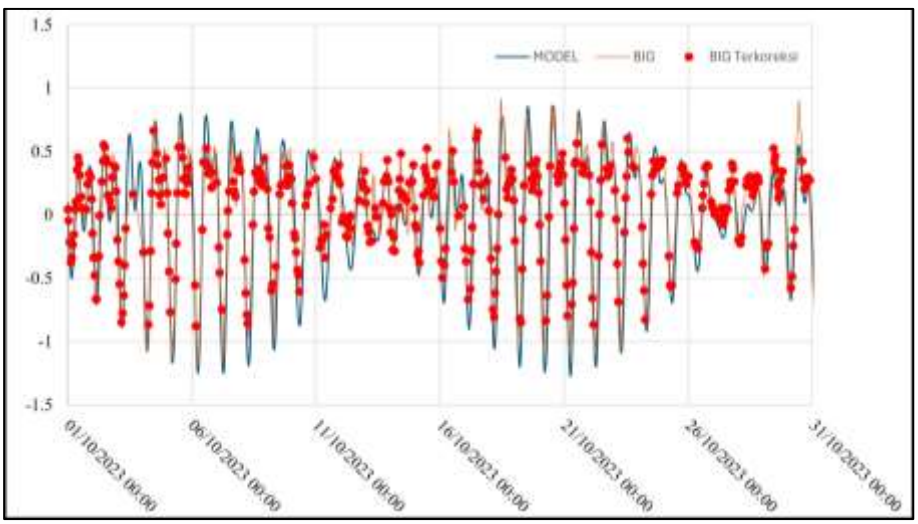

Fig. 13. Comparison of Model and Measurement Water Level Results. St. MBTN October. r=0.91, RMSE=0.182, MAPE= 1.527 %

The validation results of the hydrodynamic model against tidal data from the Pelaihari (PLHR) and Marabatuan (MBTN) stations indicate a strong agreement, with correlation coefficients ranging from 0.90 to 0.91, low RMSE values (minimum of 0.182), and acceptable MAPE percentages. These metrics demonstrate that the model effectively simulates water surface

elevation, capturing tidal dynamics with high accuracy. The results suggest that the hydrodynamic model is reliable and robust for representing the tidal phenomena in the study area during the specified period.

3.5 Current Patterns and Water Elevation Changes

During both dry and wet seasons, water elevation changes were analyzed for maximum high tide and minimum low tide conditions. Current vectors were combined to illustrate tidal flow directions, which are presented in detailed model views. The results revealed significant insights into the relationship between river water elevation at the estuary and tidal phenomena, particularly the influence of tidal currents on flow patterns.

The tidal currents, driven by the interaction of gravitational forces from the moon and sun, play a critical role in shaping the water elevation and flow dynamics in the estuarine region. During high tide, the tidal currents push water upstream into the river, raising the water elevation significantly in the estuarine area. This phenomenon, known as the tidal backwater effect, temporarily reverses the direction of flow, causing river water to move upstream. Such a reversal of flow direction impacts not only the elevation but also the sediment transport and deposition patterns within the estuary. In contrast, during low tide, the tidal currents change direction, flowing downstream toward the sea. This downstream flow reduces the water elevation in the estuary, facilitating the outflow of river water and suspended materials into the open ocean.

Figures 14–17 clearly depict the alternating flow patterns caused by tidal currents under both maximum high tide and minimum low tide conditions. The current vectors in these figures illustrate the dynamic interplay between tidal forces and riverine discharge, showing strong upstream-directed currents during high tide and downstream-directed currents during low tide. These interactions highlight the dual influence of tidal elevation changes and tidal currents in governing the hydrodynamic behavior of the estuarine system. Furthermore, the analysis underscores the importance of understanding these processes for accurate hydrodynamic and sediment transport modeling, as they directly affect sedimentation rates, erosion patterns, and water quality in the estuary and its surrounding waters.

By examining the water elevation changes and tidal current patterns during different tidal conditions, this study provides a comprehensive understanding of the complex interactions in the estuary. The findings contribute to the broader understanding of tidal hydrodynamics, emphasizing the critical role of tidal currents in regulating water elevation and flow direction within estuarine systems. These interactions and their implications can be observed in detail in Figures 14–17.

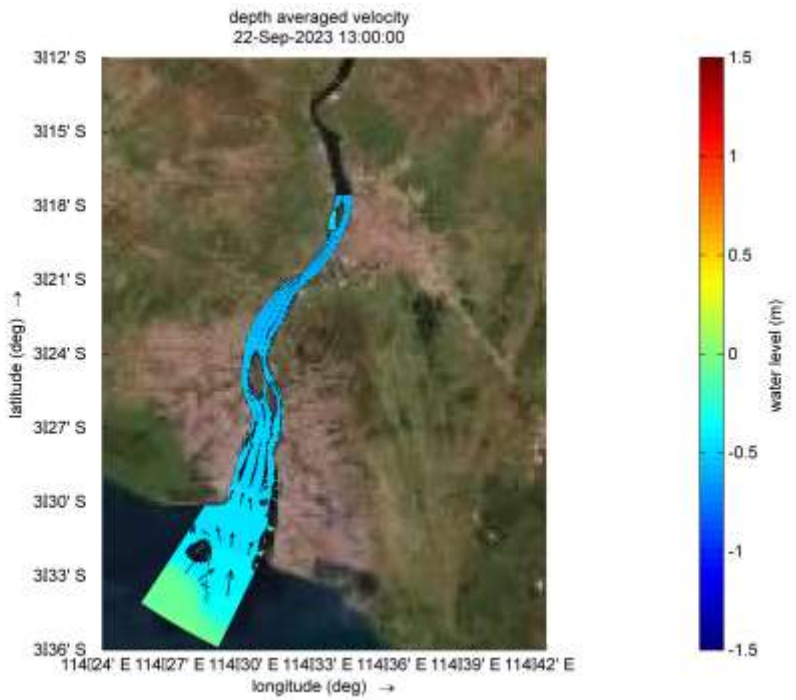

Fig. 14. Highest tidal water level in dry season model details

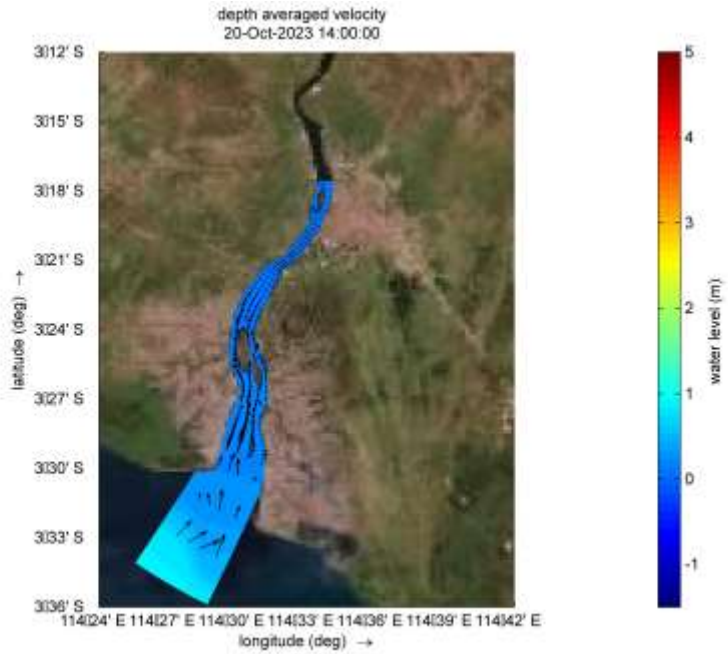

Fig. 15. Highest tidal water level in wet season model details

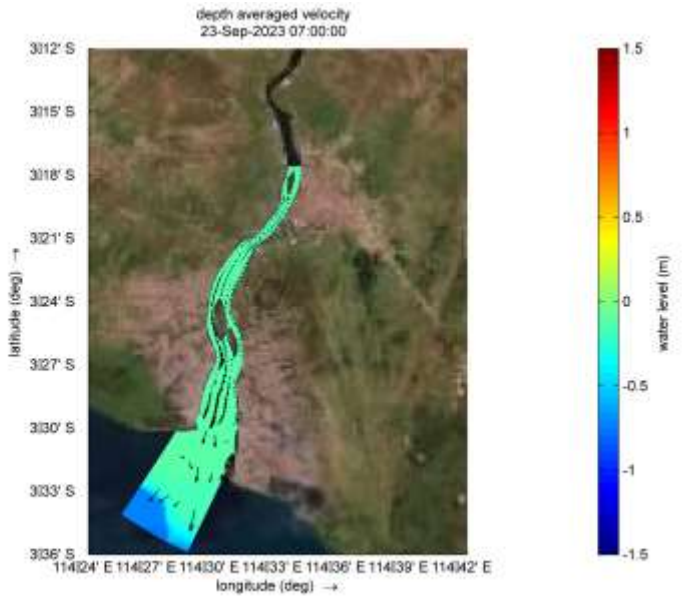

Fig. 16. Lowest low tide water level in dry season model details.

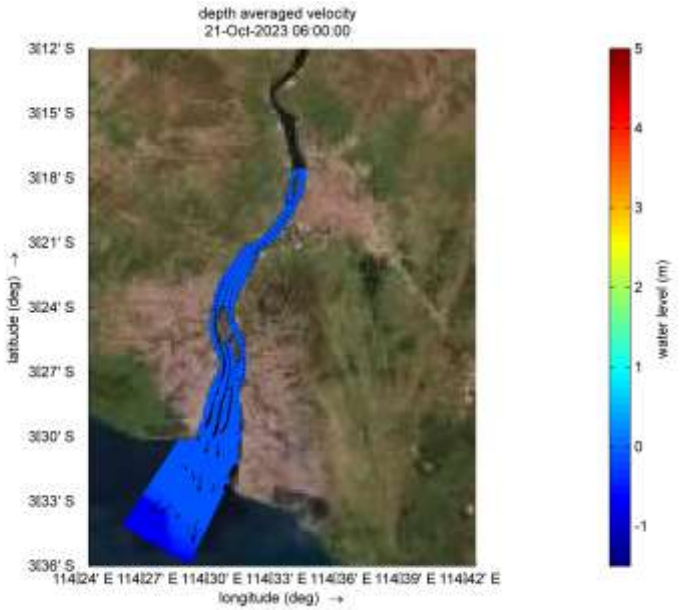

Fig. 17. Lowest low tide water level in wet season model details.

Current speed during both the dry and wet seasons was analyzed under maximum high tide and minimum low tide conditions. The analysis includes detailed representations of current speed distributions, combined with vector overlays to illustrate flow directions. These visualizations provide insights into the variability of current speeds influenced by tidal dynamics during different seasonal conditions.

3.6 Sediment Distribution Patterns

The sedimentation pattern modeling was conducted for both dry and wet season conditions, as illustrated in Figures 18 and 19, focusing on the detailed model view. The results show that during the dry season, sedimentation levels are approximately 0.1 m, while in the wet season, sedimentation levels decrease to around 0.06 m. These differences highlight the significant role of seasonal variations in influencing sediment dynamics in the estuarine region. The interplay between river discharge and current strength determines how sediment is transported and deposited, creating distinct patterns for each season.

During the dry season, the reduced river discharge and weaker currents lead to higher sediment accumulation near the estuary. The weaker currents are unable to carry sediment far from the river mouth, causing the suspended particles to settle more rapidly. This process results in the formation of sediment deposits around the estuary, contributing to greater sedimentation in this period. Such patterns are often observed in estuarine systems where dry-season flows are insufficient to effectively flush sediments out of the river mouth.

In contrast, the wet season brings increased river discharge and stronger currents, which play a critical role in reducing sedimentation near the estuary. The higher energy of the flow during this period enables sediments to be transported farther from the estuary, dispersing the particles over a wider area. This results in lower sediment accumulation near the river mouth. Similar findings have been reported in the study of hydrodynamic conditions and sediment transport in the Ayung River Estuary using Delft 3D simulations, where dry-season conditions were associated with greater sedimentation due to weaker currents and limited sediment transport. These observations reinforce the importance of seasonal dynamics in shaping sedimentation patterns in estuarine environments.

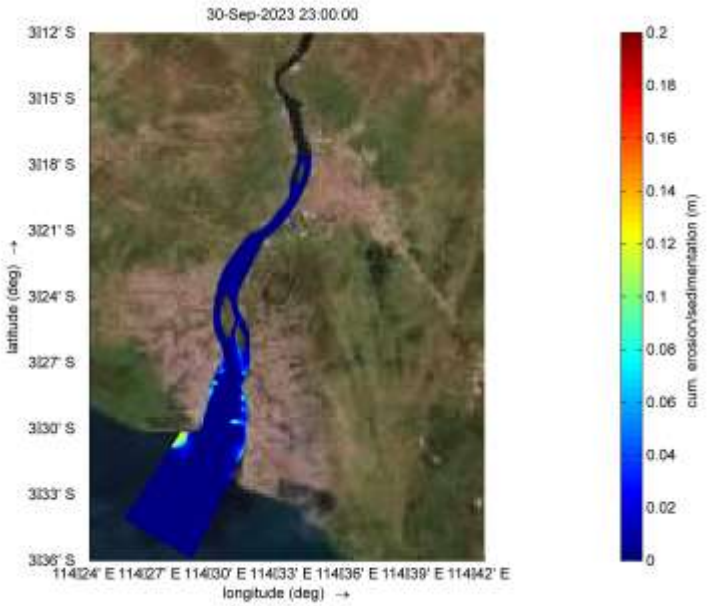

Fig. 18. Cumulative Erosion and Sedimentation Conditions During the Dry Season

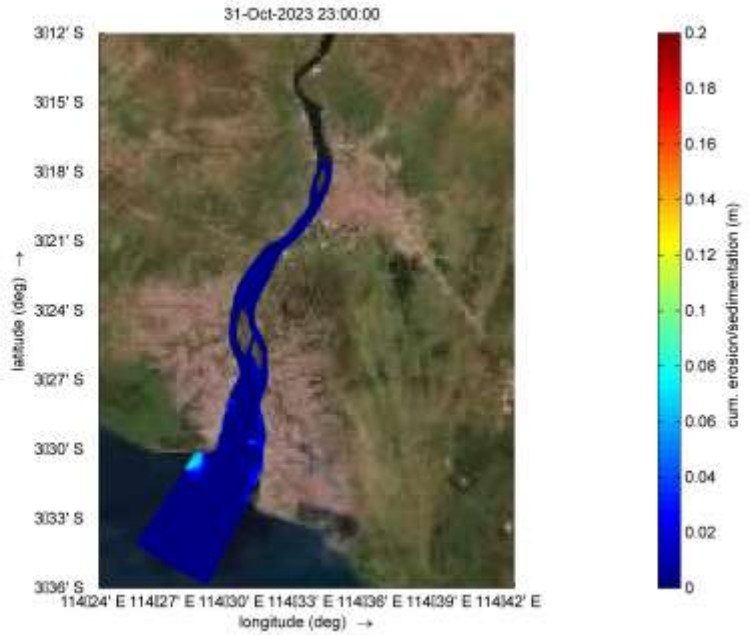

Fig. 19. Cumulative Conditions of Erosion and Sedimentation During the Wet Season

4 Conclusion

This research aimed to model current and sedimentation patterns in the Barito River Estuary, South Kalimantan, and analyze their impacts on navigation routes during wet and dry seasons. The current distribution pattern in the Barito River Estuary is influenced by river discharge and tidal conditions. During the wet season, the river discharge tends to increase due to higher

rainfall, resulting in stronger and more dominant currents. In contrast, during the dry season, river discharge decreases, and the currents are more influenced by tidal fluctuations. The hydrodynamic model shows significant variations in current speed and direction between the ebb and flow periods, as well as between the wet and dry seasons. The stronger currents during the wet season flow from upstream to downstream at higher speeds compared to the dry season. The average current speed in the model is 0.1 m/s. The validation results, with an r value of 0.91, RMSE of 0.182, and MAPE of 1.527%, indicate that the model accurately visualizes hydrodynamic events.

The sedimentation distribution pattern in the Barito River Estuary is greatly influenced by river currents and tidal conditions. During the dry season, weaker currents lead to more sediment accumulation at the estuary, as the sediment carried by the current does not travel far and settles more quickly. Conversely, during the wet season, stronger currents carry the sediment farther from the estuary, causing lower sedimentation around the estuary. The sedimentation model shows higher sediment concentrations at the estuary during the dry season. In the wet season, sedimentation is more evenly distributed and not concentrated in any particular area, as the stronger currents spread the sediment more widely. In the dry season simulation, sedimentation that may occur is approximately 0.100 m over 6 months, or about 0.017 m per month. In the wet season, sedimentation that may occur is around 0.060 m over 6 months, or about 0.010 m per month.

The changing patterns of currents and sedimentation between the wet and dry seasons have a significant impact on the navigation channels in the Barito River Estuary. During the dry season, increased sedimentation can narrow and shallow the navigation channels, reducing the depth accessible to large vessels and increasing the risk of grounding. During the wet season, although the currents are stronger, the more even sediment distribution reduces the risk of sediment accumulation in a single location. Field data analysis and modeling show that sediment accumulation during the dry season can hinder navigation and require regular dredging to maintain the channel depth. During the wet season, the navigation channels are relatively more stable and safer, although ongoing monitoring of current and sedimentation changes is still necessary.

Acknowledgement

The authors gratefully acknowledge financial support from the Institut Teknologi Sepuluh Nopember for this work, under the project scheme of the Publication Writing and IPR Incentive Program (PPHKI) 2025. The authors would also like to thank the Geospatial Information Agency (BIG) for providing the tidal data used in the model verification for this study.

References

[1] K. Sirang, “Inventarisasi dan Identifikasi Tambang di Kabupaten Murung Raya DAS Barito Hulu,” *Jurnal Hutan Tropis*, vol. 12, no. 31, pp. 44–48, 2011.
[2] E. Susilowati, “Peranan Jaringan Sungai sebagai Jalur Perdagangan di Kalimantan Selatan pada Paroh Kedua Abad XIX,” *Jurnal Sejarah Citra Lekha*, vol. 15, no. 1, 2011.
[3] Syaefudin, “Studi Pemilihan Lokasi Alternatif Pelabuhan Trisakti Banjarmasin Propinsi Kalimantan Selatan,” *Jurnal Hidrosfir Indonesia* , vol. 3, no. No.3, pp. 113–122, Dec. 2008.
[4] K. R. Munandar, Muzahar, and A. Pratomo, “Karakteristik Sedimen Di Periran Desa Tanjung Momong Kecamatan Siantan Kabupaten Kepulauan Anambas,” 2013.
[5] Ahmadi, F. Muldiyatno, and B. w, “Model Pengelolaan Alur Pelayaran Sungai Barito dengan Pendekatan Sistem Dinamik,” *JURNAL ASRO*, 2016.
[6] Kemenhub RI, *Keputusan Mentri Perhubungan RI No: KM 46 Tahun 2023 tentang Penetapan Batas-batas Penetapan Perairan Wajib Pandu Kelas 1 Pada Perairan Pelabuhan Banjarmasin Provinsi Kalimantan Selatan, Keputusan Menteri Perhubungan Republik Indonesia*. Indonesia, 2023, pp. 1–8.
[7] B. Triatmodjo, *Teknik Pantai*. Yogyakarta: Beta Offset Yogyakarta, 1999.
[8] M. F. D. Puteri, Y. S. Putra, and R. Adriat, “Penentuan Debit Aliran di Muara Sungai Pawan Kabupaten Ketapang berdasarkan Parameter Kecepatan Arus dan Kedalaman Sungai,” *PRISMA FISIKA*, vol. 7, no. 3, 2020, doi: 10.26418/pf. v7i3.38939.
[9] A. Norhadi, A. Marzuki, L. Wicaksono, and R. Addetya Yacob, “Studi Debit Aliran pada Sungai Antasan Kelurahansungai Andai Banjarmasin Utara,” *Jurnal Poros Teknik*, vol. 7, no. 1, 2015.
[10] Alpiannur, Rahman Abdur, and Rahman Mijani, “Daya Tampung Beban Pencemaran di Daerah Aliran Sungai Barito (Sub Daerah Aliran Sungai Nagara, Sub Daerah Aliran Sungai Marabhan dan Sub Derah Aliran Sungai Kuin) Provinsi Kalimantan Selatan,” *AQUATIC*, vol. 5, no. No.1, pp. 1–15, Jun. 2022.
[11] S. Kadir, *Karakteristik Daerah Aliran Sungai (DAS) Tabunio untuk merumuskan dan mengevaluasi dinamika kerentanan lingkungan*, vol. 6, no. August. 2021.
[12] Poerbandono and E. Djunarsjah, *Survei Hidrografi*. Bandung: Refika Aditama Bandung, 2005.
[13] Y. Oktavia, J. Pratama, and Apriansyah, “Estimasi Arus Laut Permukaan Yang Dibangkitkan Oleh Angin Di Perairan Indonesia,” *Prisma Fisika*, vol. VI, no. 1, 2018.

[14] Deltares, *Delft3D-FLOW Manual: Simulation of multi-dimensional hydrodynamic flows and transport phenomena, including sediments*, 4.05. Netherlands: Deltares, 2023.
[15] Y. K. Saheed, R. M. Ayobami, and T. Orje-Ishegh, "A Comparative Study of Regression Analysis for Modelling and Prediction of Bitcoin Price," in *EAI/Springer Innovations in Communication and Computing*, 2022. doi: 10.1007/978-3-030-89546-4_10.
[16] Irma Nurvianti, Budi Darma Setiawan, and Fitra Abdurrachman Bachtiar, "Perbandingan Peramalan Jumlah Penumpang Keberangkatan Kereta Api di DKI Jakarta Menggunakan Metode Double Exponential Smoothing dan Triple Exponential Smoothing," *Jurnal Pengembangan Teknologi Informasi dan Ilmu Komputer*, vol. 3, pp. 5257–5263, Jun. 2019.
[17] E. D. Kartiningrum, H. Basuki, N. Bambang, W. Otok, E. Nurul, and K. E. Yuswatiningsih, *Aplikasi Regresi Dan Korelasi Dalam Analis Data Hasil Penelitian*. 2022.
[18] B. Susetyo, *Statistika Untuk Analisis Data Penelitian*, vol. 2. 2017.
[19] Putu Indah Dianti Putri and Muhammad Syahril Badri Kusuma, "Kondisi Hidrodinamika dan Transpor Sedimen di Perairan Muara Sungai Ayung dengan Simulasi Delft 3D," *Jurnal Aplikasi Teknik Sipil*, vol. 21, no. No.4, Nov. 2023.